First Constraints on the Epoch of Reionization Using the Non-Gaussianity of the Kinematic Sunyaev-Zel'dovich Effect from the South Pole Telescope and Herschel-SPIRE Observations

S. Raghunathan,[1] P. A. R. Ade,[2] A. J. Anderson,[3,4,5] B. Ansarinejad,[6] M. Archipley,[7,1] J. E. Austermann,[8,9] L. Balkenhol,[10] J. A. Beall,[8] K. Benabed,[10] A. N. Bender,[11,4,5] B. A. Benson,[3,4,5] F. Bianchini,[12,13,14] L. E. Bleem,[11,4,5] J. Bock,[15,16] F. R. Bouchet,[10] L. Bryant,[17] E. Camphuis,[10] J. E. Carlstrom,[4,17,18,11,5] T. W. Cecil,[11] C. L. Chang,[11,4,5] P. Chaubal,[6] H. C. Chiang,[19,20] P. M. Chichura,[18,4] T.-L. Chou,[18,4] R. Citron,[21] A. Coerver,[22] T. M. Crawford,[4,5] A. T. Crites,[4,5,23,24] A. Cukierman,[12,14,13] C. Daley,[7] K. R. Dibert,[5,4] M. A. Dobbs,[19,25] A. Doussot,[10] D. Dutcher,[26] W. Everett,[27] C. Feng,[28] K. R. Ferguson,[29] K. Fichman,[18,4] A. Foster,[26] S. Galli,[10] J. Gallicchio,[4,30] A. E. Gambrel,[4] R. W. Gardner,[17] F. Ge,[31] E. M. George,[32,22] N. Goeckner-Wald,[13,12] R. Gualtieri,[33] F. Guidi,[10] S. Guns,[22] N. Gupta,[34] T. de Haan,[35] N. W. Halverson,[36,9] E. Hivon,[10] G. P. Holder,[28] W. L. Holzapfel,[22] J. C. Hood,[4] J. D. Hrubes,[21] A. Hryciuk,[18,4] N. Huang,[22] J. Hubmayr,[8] K. D. Irwin,[14,13] F. Kéruzoré,[11] A. R. Khalife,[10] L. Knox,[31] M. Korman,[37] K. Kornoelje,[5,4] C.-L. Kuo,[12,13,14] A. T. Lee,[22,38] K. Levy,[6] D. Li,[8,14] A. E. Lowitz,[4] C. Lu,[28] A. Maniyar,[12,13,14] E. S. Martsen,[5,4] J. J. McMahon,[4,18,5] F. Menanteau,[7,1] M. Millea,[22] J. Montgomery,[19] C. Corbett Moran,[39] Y. Nakato,[13] T. Natoli,[4] J. P. Nibarger,[8] G. I. Noble,[40,24] V. Novosad,[41] Y. Omori,[5,4] S. Padin,[4,42] Z. Pan,[11,4,18] P. Paschos,[17] S. Patil,[6] K. A. Phadke,[7,1] K. Prabhu,[31] C. Pryke,[43] W. Quan,[18,4] M. Rahimi,[6] A. Rahlin,[3,4] C. L. Reichardt,[6] M. Rouble,[19] J. E. Ruhl,[37] B. R. Saliwanchik,[44] K. K. Schaffer,[4,17,45] E. Schiappucci,[6] C. Sievers,[21] G. Smecher,[46] J. A. Sobrin,[3,4] A. A. Stark,[47] J. Stephen,[17] A. Suzuki,[38] C. Tandoi,[7] K. L. Thompson,[12,13,14] B. Thorne,[31] C. Trendafilova,[1] C. Tucker,[2] C. Umilta,[28] T. Veach,[48] J. D. Vieira,[7,28,1] M. P. Viero,[15] Y. Wan,[7,1] G. Wang,[11] N. Whitehorn,[49] W. L. K. Wu,[12,14] V. Yefremenko,[11] M. R. Young,[3,4] J. A. Zebrowski,[4,5,3] and M. Zemcov[50,16]

(SPT-3G and SPTpol Collaboration)

[1]*Center for AstroPhysical Surveys, National Center for Supercomputing Applications, Urbana, Illinois 61801, USA*
[2]*School of Physics and Astronomy, Cardiff University, Cardiff CF24 3YB, United Kingdom*
[3]*Fermi National Accelerator Laboratory, MS209, P.O. Box 500, Batavia, Illinois 60510, USA*
[4]*Kavli Institute for Cosmological Physics, University of Chicago, 5640 South Ellis Avenue, Chicago, Illinois 60637, USA*
[5]*Department of Astronomy and Astrophysics, University of Chicago, 5640 South Ellis Avenue, Chicago, Illinois 60637, USA*
[6]*School of Physics, University of Melbourne, Parkville, Victoria 3010, Australia*
[7]*Department of Astronomy, University of Illinois Urbana-Champaign, 1002 West Green Street, Urbana, Illinois 61801, USA*
[8]*NIST Quantum Devices Group, 325 Broadway Mailcode 817.03, Boulder, Colorado 80305, USA*
[9]*Department of Physics, University of Colorado, Boulder, Colorado 80309, USA*
[10]*Institut d'Astrophysique de Paris, UMR 7095, CNRS and Sorbonne Université, 98 bis boulevard Arago, 75014 Paris, France*
[11]*High-Energy Physics Division, Argonne National Laboratory, 9700 South Cass Avenue, Lemont, Illinois 60439, USA*
[12]*Kavli Institute for Particle Astrophysics and Cosmology, Stanford University, 452 Lomita Mall, Stanford, California 94305, USA*
[13]*Department of Physics, Stanford University, 382 Via Pueblo Mall, Stanford, California 94305, USA*
[14]*SLAC National Accelerator Laboratory, 2575 Sand Hill Road, Menlo Park, California 94025, USA*
[15]*California Institute of Technology, Pasadena, California 91125, USA*
[16]*Jet Propulsion Laboratory, California Institute of Technology, Pasadena, California 91109, USA*
[17]*Enrico Fermi Institute, University of Chicago, 5640 South Ellis Avenue, Chicago, Illinois 60637, USA*
[18]*Department of Physics, University of Chicago, 5640 South Ellis Avenue, Chicago, Illinois 60637, USA*
[19]*Department of Physics and McGill Space Institute, McGill University, 3600 Rue University, Montreal, Quebec H3A 2T8, Canada*
[20]*School of Mathematics, Statistics and Computer Science, University of KwaZulu-Natal, Durban, South Africa*
[21]*University of Chicago, 5640 South Ellis Avenue, Chicago, Illinois 60637, USA*
[22]*Department of Physics, University of California, Berkeley, California 94720, USA*
[23]*Dunlap Institute for Astronomy and Astrophysics, University of Toronto, 50 St. George Street, Toronto, Ontarios M5S 3H4, Canada*
[24]*David A. Dunlap Department of Astronomy and Astrophysics, University of Toronto, 50 St. George Street, Toronto, Ontario M5S 3H4, Canada*
[25]*Canadian Institute for Advanced Research, CIFAR Program in Gravity and the Extreme Universe, Toronto, Ontario M5G 1Z8, Canada*
[26]*Joseph Henry Laboratories of Physics, Jadwin Hall, Princeton University, Princeton, New Jersey 08544, USA*
[27]*Department of Astrophysical and Planetary Sciences, University of Colorado, Boulder, Colorado 80309, USA*
[28]*Department of Physics, University of Illinois Urbana-Champaign, 1110 West Green Street, Urbana, Illinois 61801, USA*

[29]Department of Physics and Astronomy, University of California, Los Angeles, California 90095, USA
[30]Harvey Mudd College, 301 Platt Boulevard., Claremont, California 91711, USA
[31]Department of Physics and Astronomy, University of California, One Shields Avenue, Davis, California 95616, USA
[32]European Southern Observatory, Karl-Schwarzschild-Str. 2, 85748 Garching bei München, Germany
[33]Department of Physics and Astronomy, Northwestern University, 633 Clark St., Evanston, Illinois 60208, USA
[34]CSIRO Space and Astronomy, PO Box 1130, Bentley, Western Australia 6102, Australia
[35]High Energy Accelerator Research Organization (KEK), Tsukuba, Ibaraki 305-0801, Japan
[36]CASA, Department of Astrophysical and Planetary Sciences, University of Colorado, Boulder, Colorado 80309, USA
[37]Department of Physics, Case Western Reserve University, Cleveland, Ohio 44106, USA
[38]Physics Division, Lawrence Berkeley National Laboratory, Berkeley, California 94720, USA
[39]Jet Propulsion Laboratory, Pasadena, California 91109, USA
[40]Dunlap Institute for Astronomy and Astrophysics, University of Toronto, 50 St. George Street, Toronto, Ontario M5S 3H4, Canada
[41]Materials Sciences Division, Argonne National Laboratory, 9700 South Cass Avenue, Lemont, Illinois 60439, USA
[42]California Institute of Technology, 1200 East California Boulevard., Pasadena, California 91125, USA
[43]School of Physics and Astronomy, University of Minnesota, 116 Church Street SE Minneapolis, Minnesota 55455, USA
[44]Instrumentation Division, Brookhaven National Laboratory, Upton, New York 11973, USA
[45]Liberal Arts Department, School of the Art Institute of Chicago, 112 South Michigan Avenue, Chicago, Illinois 60603, USA
[46]Three-Speed Logic, Inc., Victoria, British Columbia V8S 3Z5, Canada
[47]Harvard-Smithsonian Center for Astrophysics, 60 Garden Street, Cambridge, Massachusetts 02138, USA
[48]Space Science and Engineering Division, Southwest Research Institute, San Antonio, Texas 78238, USA
[49]Department of Physics and Astronomy, Michigan State University, East Lansing, Michigan 48824, USA
[50]School of Physics and Astronomy, Rochester Institute of Technology, Rochester, New York 14623, USA

(Received 7 March 2024; revised 6 June 2024; accepted 15 August 2024; published 19 September 2024)

We report results from an analysis aimed at detecting the trispectrum of the kinematic Sunyaev-Zel'dovich (kSZ) effect by combining data from the South Pole Telescope (SPT) and *Herschel*-SPIRE experiments over a 100 deg^2 field. The SPT observations combine data from the previous and current surveys, namely SPTpol and SPT-3G, to achieve depths of 4.5, 3, and 16 μK-arcmin in bands centered at 95, 150, and 220 GHz. For SPIRE, we include data from the 600 and 857 GHz bands. We reconstruct the velocity-induced large-scale correlation of the small-scale kSZ signal with a quadratic estimator that uses two cosmic microwave background (CMB) temperature maps, constructed by optimally combining data from all the frequency bands. We reject the null hypothesis of a zero trispectrum at 10.3σ level. However, the measured trispectrum contains contributions from both the kSZ and other undesired components, such as CMB lensing and astrophysical foregrounds, with kSZ being sub-dominant. We use the AGORA simulations to estimate the expected signal from CMB lensing and astrophysical foregrounds. After accounting for the contributions from CMB lensing and foreground signals, we do not detect an excess kSZ-only trispectrum and use this nondetection to set constraints on reionization. By applying a prior based on observations of the Gunn-Peterson trough, we obtain an upper limit on the duration of reionization of $\Delta z_{\mathrm{re},50} < 4.5$ (95% confidence level). We find these constraints are fairly robust to foregrounds assumptions. This trispectrum measurement is independent of, but consistent with, Planck's optical depth measurement. This result is the first constraint on the epoch of reionization using the non-Gaussian nature of the kSZ signal.

DOI: 10.1103/PhysRevLett.133.121004

Introduction—The kinematic Sunyaev-Zel'dovich (kSZ) effect originates when electrons with bulk motion Compton-scatter cosmic microwave background (CMB) photons [1]. Detecting the kSZ signal can provide crucial insights on both structure formation [2,3] and the physics of reionization [4–9]. This is because the source of the kSZ signal can be decomposed into two main categories: a low-redshift ($z \lesssim 3$) component referred to as homogeneous or postreionization kSZ and a high-redshift ($z \gtrsim 6$) component referred to as inhomogeneous or reionization kSZ. The postreionization kSZ signal is due to the bulk flow of halos with free electrons in the local universe. The reionization kSZ, on the other hand, is due to motion of the ionized bubbles containing free electrons during the epoch of reionization (EoR). Several observations [e.g., [10–12]] suggest that the energetic ultraviolet light from the first stars and galaxies at $z \gtrsim 6$ was responsible for ionizing the neutral hydrogen in the early Universe, although more data is required to precisely understand the process, timing, and duration of the EoR [13]. From the CMB data, besides kSZ, the EoR can also be probed using the large-scale bump in the CMB EE/TE power spectra [14]. Measurements of the

large-scale ($\ell \lesssim 10$) modes from ground-based experiments, because of the limited sky coverage, will be dominated by the sample variance that reduces the sensitivity to the low-ℓ EE/TE reionization bump. In addition to this, the low-ℓ bump is not sensitive to the details of the process of reionization and cannot distinguish between different reionization histories (see Fig. 4 of [15]. Hence, it is important to explore other probes of EoR, like the kSZ.

The kSZ signals are subdominant compared to other signals in maps of total intensity and detecting them has proven to be challenging. In the past, the kSZ signals have been detected through cross-correlation of CMB maps with galaxy surveys [16–21] but these measurements only probe the postreionization kSZ signal. Although cross-correlations with high-redshift galaxy catalogs are in principle possible for the reionization kSZ, the expected signal to noise (SNR) is small (2–3σ) even for future Stage-4 experiments because of the difficulty in obtaining galaxy catalogs at $z \gtrsim 6$ [22]. Hence, forecasts for kSZ constraints on the EoR have typically relied on kSZ power spectrum (2-point correlation) measurements or reconstructions of the optical depth [23]. The kSZ 2-point function, however, receives contributions from both of the kSZ components and disentangling the two is difficult due to their similar shapes and amplitudes [24,25]. The presence of astrophysical foregrounds in the CMB maps, especially thermal SZ (tSZ) and cosmic infrared background (CIB) signals, complicates the interpretation of the kSZ power spectrum further as these foreground signals are much brighter than kSZ [26] (hereafter, [RO23]). As a result, EoR constraints from recent measurements of the total kSZ power spectrum [27,28] have been limited by knowledge of the foreground and postreionization kSZ signal.

Smith and Ferraro [29] (hereafter [SF17]) proposed a novel method of using the kSZ trispectrum (4-point function) to probe the physics of reionization (see also [30,31]). Since the reionization kSZ signal depends on both the free electron density and the velocity, the small-scale fluctuations in electron density due to inhomogeneous reionization will get modulated on larger scales by the velocity field, leading to position-dependent non-Gaussianities in the CMB maps. Thus, the kSZ non-Gaussianity arises due to the large-scale correlations of small-scale clustering of halos, similar to CMB lensing [SF17]. However, in our case the large-scale correlations are due to the bulk velocity flow in the Universe rather than due to gravitational lensing [32]. Although the postreionization kSZ also starts out as a non-Gaussian signal at different epochs, the comoving line-of-sight distance over which it gets integrated in the local universe is much larger and the signal ends up being Gaussian based on the central limit theorem. This characteristic allows the two kSZ components to be easily distinguished using the trispectrum (see Fig. 2 of [SF17]). Despite this advantage, the constraints on reionization from kSZ 4-point alone are not expected to be as competitive as the optical depth measurements from Planck, even for future CMB surveys, due to the degeneracy between the parameters that govern reionization. However, as demonstrated by Alvarez *et al.* [31], the joint constraints from kSZ 4-point, Planck primary CMB, and kSZ 2-point can effectively break that degeneracy, resulting in a significant improvement on reionization compared to what can be achieved individually by any of these probes.

In this Letter, we present results from an analysis aimed at detecting the kSZ trispectrum using CMB temperature maps obtained by combining South Pole Telescope (SPT) and Herschel-SPIRE datasets. The observed trispectrum receives a contribution from reionization kSZ but is dominated by CMB lensing and astrophysical foreground signals. We build a template for the latter using the Agora simulations [33]. Given the difficulties in correctly modeling the foreground signals and the lower amplitude of the kSZ signals compared to the other undesired signals, we adopt different strategies to handle the foregrounds. In the baseline case, we marginalize over the amplitude of the CMB lensing and foreground signals. We also take the approach of fixing the CMB lensing and foreground signals. In neither case do we observe an excess kSZ trispectrum. We use this nondetection along with a prior based on the measurements of the Gunn-Peterson (GP) trough to set upper limits (95% CL) on the duration of reionization $\Delta z_{\mathrm{re},50}$ corresponding to the difference in redshifts at which the Universe has been 25% and 75% reionized. We show that our results are consistent with Planck's optical depth measurement. We do not combine our results with the kSZ 2-point measurements from the literature [27,28] owing to assumptions made about foregrounds and the postreionization kSZ signals made in those works.

Datasets—This work uses data from two different experiments: SPT [34,35] and Herschel-SPIRE [36,37]. For SPT, we use data from two surveys: SPTpol [38] and SPT-3G [39–41]. The SPTpol observations were carried out between 2012 and 2016, and in this work we only use the 150 GHz observations [42] since the noise level of 95 GHz SPTpol is roughly 3 times higher than the equivalent SPT-3G data. The SPT-3G observations used in this work were carried out between 2019 and 2020, and we include data from all the three bands: 95, 150, and 220 GHz. After combining SPTpol and SPT-3G, the map depths for the three bands are 4.5, 3, and 16 μK-arcmin, respectively. For Herschel-SPIRE, we use the data from 600 GHz (500 μm) and 857 GHz (350 μm) bands. Since Herschel-SPIRE is primarily used for CIB mitigation and since the CIB decorrelation between SPT bands and Herschel-SPIRE's 1200 GHz (250 μm) band is high [43], we do not use the 1200 GHz band in this work. We limit the SPT footprint in this work to the region that has overlap with Herschel-SPIRE, which is a roughly 100 deg^2 region centered at $(\mathrm{RA}, \mathrm{Decl.}) = (23\ \mathrm{h}, 30\ \mathrm{min}, -55°)$. We

provide details about the data processing in Supplemental Material [44]. In short, the raw SPT data is filtered and binned into maps with a pixel resolution of 0.′5. The effect of filtering is accounted for by using the transfer function (TF) calculated from simulations. The individual frequency maps are then calibrated by cross-correlating with Planck. The SPIRE and calibrated SPT maps are combined to produce a minimum-variance (MV) map which has an unbiased response to CMB temperature. This is done using a scale-dependent linear combination (LC) technique [45], and we refer to the product as the MV-LC.

Results and discussion—We briefly describe the methods to extract reionization kSZ information from the CMB maps and refer the reader to Appendix B of Supplemental Material [44] for more details. Following the work of [SF17], we develop a quadratic estimator (QE) to reconstruct $\hat{K}(\hat{\mathbf{n}})$ that captures the degree-scale correlations of small-scale clustering of the kSZ signal. The desired kSZ trispectrum $\hat{C}_L^{KK} = \delta(L - L')\hat{K}_L\hat{K}^*_{L'}$ is the power spectrum of the reconstructed $\hat{K}(\hat{\mathbf{n}})$ map [SF17] after removing an estimate of the mean field that arises due to masking. For $\hat{C}_L^{KK}$ measurement, we set a bin width of $\Delta_L = 50$ in the range $L \in [50, 300]$. Besides the desired kSZ signal and the mean field, the reconstructed map receives contributions from the following: $\hat{N}_L^{(0,KK)}$, which is the Gaussian disconnected piece arising due to chance correlations of the two CMB maps used in the QE, and the systematics from CMB lensing and foregrounds. We use AMBER (Agora) simulations to model the reionization kSZ (CMB lensing and foregrounds) and assume a Gaussian likelihood to derive constraints on reionization.

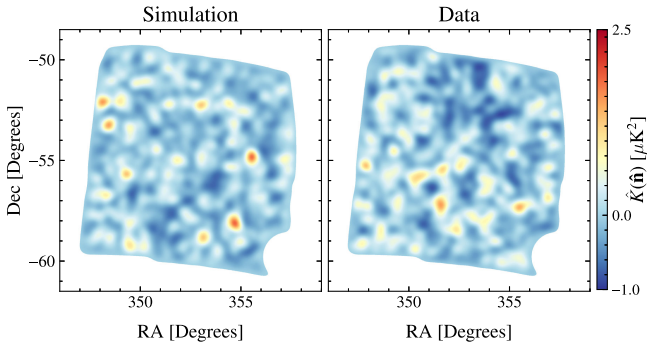

FIG. 1. Mean field subtracted $\hat{K}(\hat{\mathbf{n}})$ maps from a single simulation run in the left panel and data in the right panel. Both the panels have been smoothed using a Gaussian beam with $\theta_{\rm FWHM} = 30'$. The figure illustrates that our data and simulations have qualitatively similar-looking features. The simulation only contains CMB, foregrounds, and noise. It does not include the reionization kSZ signal. The similarity of the simulation with the data map suggests that the reconstructed $\hat{K}(\hat{\mathbf{n}})$ is dominated by $\hat{N}_L^{(0,KK)}$ and foregrounds. We also provide quantitative comparison between the data and the simulations in the text.

The left panel of Fig. 1 shows the $\hat{K}(\hat{\mathbf{n}})$ reconstructed from a single non-Gaussian simulation run while the right panel is for data. We note that the statistical properties look qualitatively similar between the panels. The simulation includes CMB, foregrounds, and noise but does not contain the reionization kSZ signal. The similarity between the simulation and data suggests that our reconstructed $\hat{K}(\hat{\mathbf{n}})$ should be dominated by $\hat{N}_L^{(0,KK)}$ and foregrounds, and the kSZ signal must be subdominant.

In Fig. 2 we present the $\hat{C}_L^{KK}$ measurements from simulations and data. These correspond to the results with our fiducial filter choices $(\ell_{\rm min}, \ell_{\rm max}) = (3300, 4300)$ in Eq. (1) of Supplemental Material [44]. The result from data (green circles) is consistent with the distribution of the simulations represented by the violins. With our data, we reject the null hypothesis of a zero trispectrum at 10.3σ. This raw SNR has been calculated just with the Gaussian covariance $\hat{\mathbf{\Sigma}}^{KK}_{\rm Gau}$ (see Eq. (5) of the Supplemental Material [44]). The mean of all the simulations, which we use as the estimate of $\hat{C}^{KK}_{L,\rm sys}$ is the black solid curve. The semitransparent band around the mean is the systematic uncertainty in $\hat{C}^{KK}_{L,\rm sys}$ obtained by scaling the tSZ signal in the input simulations by $\pm 20\%$ roughly consistent with the uncertainty in the hydrostatic mass bias parameter [66]. The impact of this systematic on our constraints is presented in Fig. 3 (and in Fig. 2 of the Supplemental Material [44]). The change in the results is only marginal if we scaled the CIB instead of the tSZ. The blue dash-dotted curve is $\hat{N}_L^{(0,KK)}$ calculated using 250 simulations, and it has been removed from all the other curves in the figure. The error bars include contribution both from the scatter in the Gaussian $\hat{N}_L^{(0,KK)}$ and the non-Gaussian signals. For reference, we also show the expected kSZ 4-point function signal in shades of orange. These assume a fixed midpoint $z_{\rm re}^{\rm mid} = 7.69$ and different values of duration $\Delta z_{\rm re,50} \in [1, 15]$.

The probability to exceed (p value), obtained by comparing the individual simulations (distributions shown using the violins) and data (green) with the $\hat{C}^{KK}_{L,\rm sys}$ template (black) and computing $p = \chi^2_{\rm sims} \geq \chi^2_{\rm data}$ is $p = 0.23$, indicating the consistency between the data and the simulations. Note that, similar to Fig. 1, the simulations do not include the reionization kSZ signal. This suggests that the reionization kSZ signal must be subdominant compared to $\hat{N}_L^{(0,KK)}$ and 4-point function contributions from CMB lensing and foregrounds $\hat{C}^{KK}_{L,\rm sys}$. Indeed, when we remove the $\hat{C}^{KK}_{L,\rm sys}$ estimate from data, the residual $\hat{C}_L^{KK}$ measurement is consistent with a null signal with $p = 0.39$.

Reionization constraints—We compare the $\hat{C}_L^{KK}$ measurements obtained above to the expected kSZ signal from AMBER to place constraints on the EoR parameters. We fit for three parameters ($z_{\rm re}^{\rm mid}$, $\Delta z_{\rm re,50}$, and $A_{\rm CMB-FG}$) where

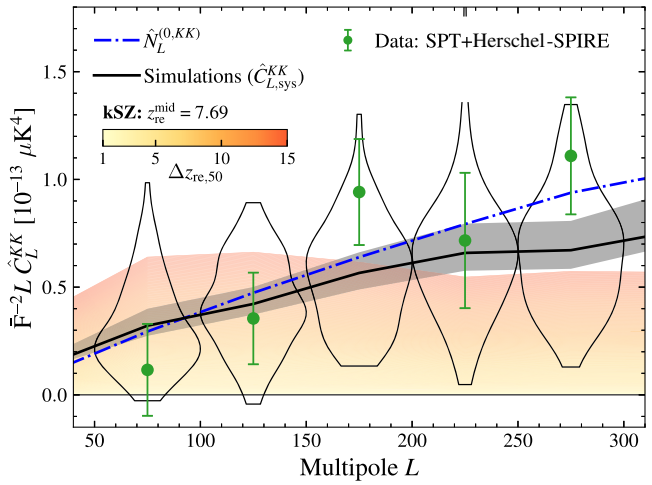

FIG. 2. Reconstructed $\hat{C}_L^{KK}$ signals. The violins represent the scatter in the measurements from the 100 non-Gaussian (reionization kSZ-free) simulations in each L bin and green data points represent data. The mean of all the simulations ($\hat{C}_{L,\rm sys}^{KK}$) is shown in black. The band around the black curve indicates the systematic uncertainty in the template obtained by scaling the tSZ signal in the input simulations by $\pm 20\%$. For each curve, the estimate of $\hat{N}_L^{(0,KK)}$ (blue dash-dotted curve) has been removed. For reference, we also show the expected kSZ signal from AMBER simulations for $z_{\rm re}^{\rm mid} = 7.69$ and different values of $\Delta z_{\rm re,50}$ in shades of orange. From the figure, it is evident that the data are consistent with the non-Gaussian simulations, which do not contain any reionization kSZ signal, in agreement with the $\hat{K}(\hat{\mathbf{n}})$ maps in Fig. 1.

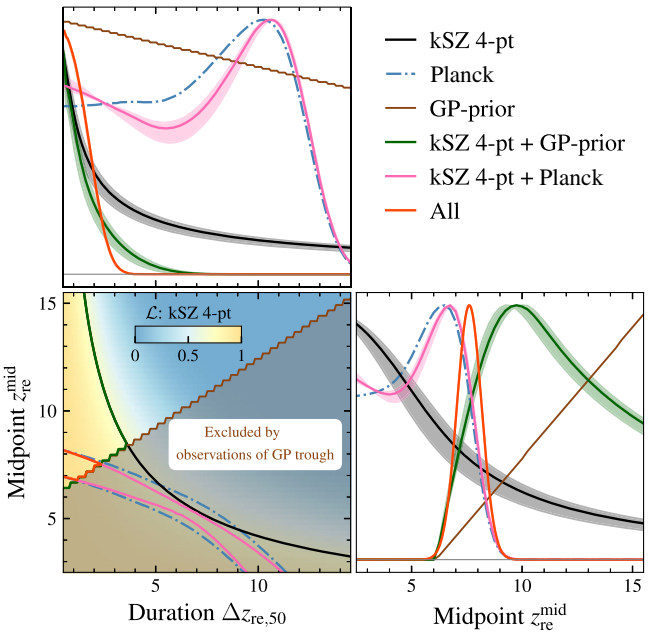

FIG. 3. Constraints on EoR parameters ($\Delta z_{\rm re,50}$ and $z_{\rm re}^{\rm mid}$) for different dataset combinations after marginalizing over $A_{\rm CMB-FG}$ (FG represents foreground). We present both 2D and 1D posteriors. The two parameters are highly degenerate for kSZ 4-point alone, as shown in the 2D posterior plot. The black line represents the 68% CL joint upper limit to the two parameters in the 2D plot and the marginalized one-parameter posteriors in the 1D plots. The green lines show the analogous curves after applying a prior based on GP trough measurements that removes regions where reionization ends later than $z = 6$. For reference, the GP prior is shown in brown. We adopt these as our baseline constraints, and for this case we set a 95% CL upper limit of $\Delta z_{\rm re,50} < 4.5$. We also show 68% CL allowed 2D regions and 1D posterior curves derived from Planck's low-ℓ optical depth measurement (blue dash-dotted curve) and from combining Planck and kSZ 4-point with (without) the GP-based prior in red (pink). The band around the combinations that include kSZ 4-point data represents the uncertainties in $\hat{C}_{L,\rm sys}^{KK}$ template. To avoid cluttering, we show the band only in the 1D posteriors.

$A_{\rm CMB-FG}$ is the amplitude term for the Agora $\hat{C}_{L,\rm sys}^{KK}$ template. In Supplemental Material [44], we use simulations to show that this approach is robust to the assumptions about the $\hat{C}_{L,\rm sys}^{KK}$ template and returns unbiased results on simulated data.

In Fig. 3, we present the constraints on $\Delta z_{\rm re,50}$ and $z_{\rm re}^{\rm mid}$ for different dataset combinations. As evident from the figure, the two parameters are degenerate for the kSZ 4-point-only case shown in the 2D posterior. On the other hand, evidence based on the measurements of GP trough [10,11] in the spectra of high-redshift quasars suggests that hydrogen in the Universe must be fully ionized by $z \sim 5$–6. We use this information to set a binary GP-based prior (brown) on the reionization histories $X_{\rm e}(z)$ from AMBER. To this end, we remove regions in the $(z_{\rm re}^{\rm mid} - \Delta z_{\rm re,50})$ plane where reionization ends later than $z < 6$ by setting their prior to zero. We define the end of reionization as the redshift at which $X_{\rm e}(z) > 0.95$. The kSZ 4-point result combined with the GP-based prior is shown in green, and we adopt this as our baseline result. For this case, we are able to set an upper limit on $\Delta z_{\rm re,50}$ of < 4.5 (95% CL). Modifying the GP-based prior to have the reionization end at $z < 5$ rather than $z < 6$ slightly increases the upper limit to $\Delta z_{\rm re,50} < 5$ (95% CL).

We also show constraints based on the Planck optical depth measurement (blue dash-dotted curve) as well as the kSZ 4-point measurement + Planck with and without the GP-based prior (pink and red curves respectively) in Fig. 3. As expected, Planck (blue) tightly constrains the upper tail of the midpoint of reionization but is not sensitive to the duration with an upper limit of $\Delta z_{\rm re,50}$ of < 13.0 (95% CL). Adding kSZ 4-point to Planck without the GP-based prior (pink) leads to marginal ($< 10\%$) changes in the results. On the other hand, by including the GP-based prior to kSZ 4 pt + Planck (red), we set an upper limit on $\Delta z_{\rm re,50}$ of < 2.6 (95% CL) and obtain $z_{\rm re}^{\rm mid} = 7.4 \pm 0.6$. This combination is dominated by Planck and the GP-based prior, and kSZ 4-point only adds marginal improvement, however, and we do not quote it as our main result.

For the amplitude of the CMB lensing and foreground template, we obtain a best-fit amplitude of $A_{\mathrm{CMB-FG}} = 1.25 \pm 0.32$. The detection significance for $A_{\mathrm{CMB-FG}}$ is consistent with what we expect from simulations shown in the inset plots of Fig. 1 of Supplemental Material [44]. As shown in Fig. 2 of the Supplemental Material [44], we do not observe a strong degeneracy between $A_{\mathrm{CMB-FG}}$ and the EoR parameters.

To summarize, we quote the constraint from kSZ 4-point with the GP-based prior (green curves in Fig. 3) as our baseline result and we set an upper limit on the duration of reionization of $\Delta z_{\mathrm{re},50} < 4.5$ (95% CL). These are the first constraints on EoR parameters using the non-Gaussianity of the kSZ signal.

Foreground uncertainties—In Fig. 3, the band around the dataset combinations that include kSZ 4-point data represents the uncertainties in $\hat{C}^{KK}_{L,\mathrm{sys}}$ propagated to uncertainties in the parameter constraints. These are obtained by scaling the tSZ signal in the simulations by 20% (semi-transparent black band around $\hat{C}^{KK}_{L,\mathrm{sys}}$ in Fig. 2). As evident from the figure, the uncertainties in $\hat{C}^{KK}_{L,\mathrm{sys}}$ have negligible effect indicating constraints are robust to assumptions about the CMB + FG template. For example, the 95% CL of $\Delta z_{\mathrm{re},50}$ changes by ∼7% when the $\hat{C}^{KK}_{L,\mathrm{sys}}$ is modified to take the uncertainties into account. The above results are for our fiducial values for $(\ell_{\mathrm{min}}, \ell_{\mathrm{max}}) = (3300, 4300)$ with $\Delta_\ell = 1000$. We find these values to be optimal both in terms of SNR and the foreground biases. In Supplemental Material [44], we justify this by discussing the changes to SNR and the impact of foregrounds when the values of $\ell_{\mathrm{min}}, \ell_{\mathrm{max}}, \Delta_\ell$ are modified. We also show the systematics due to uncertainties in beam and TF to be negligible.

Conclusion—In this Letter, we reported results from an analysis aimed at detecting the non-Gaussian nature of the kSZ signal from reionization. We combined data from SPTpol, SPT-3G, and Herschel-SPIRE surveys in a 100 deg^2 field. Using MV-LC map and a QE, we detected the total trispectrum $\hat{C}^{KK}_L$ at 10.3σ. The measurement is dominated by $\hat{N}^{(0,KK)}_L$ bias from the disconnected term, and the contributions from CMB lensing and foreground signals. After accounting for these undesired signals, we do not measure an excess kSZ trispectrum and our results are consistent with a null signal ($p = 0.39$). The results from data are consistent with the expectations from simulations ($p = 0.23$). We quantified the biases due to uncertainties in instrumental beam and TF, and found them to be negligible. We also thoroughly checked the biases due to mismatch between the Agora foreground template and data, and found that our results are robust to uncertainties in both amplitude and shape of the template.

We found that the constraints on $z^{\mathrm{mid}}_{\mathrm{re}}$ and $\Delta z_{\mathrm{re},50}$ are highly degenerate from kSZ 4-point alone. Hence, we applied a loose prior based on GP trough measurements on the reionization histories from AMBER to remove $z^{\mathrm{mid}}_{\mathrm{re}}$ and $\Delta z_{\mathrm{re},50}$ from the parameter space where the reionization ends later than $z_{\mathrm{end}} = 6$. With this prior, we set a upper limit (95% CL) of $\Delta z_{\mathrm{re},50} < 4.5$. This result is independent of, but consistent with, the optical depth measurement from Planck. This work represents the first constraints on EoR parameters using the trispectrum of the kSZ signal.

In this Letter, we have used simulations to model the contributions from lensing and foregrounds. There are other potential strategies to mitigate them at the expense of a penalty in SNR. These include bias hardening [67–69] and delensing [70,71], which might be particularly relevant for the future surveys and should be explored further. Furthermore, we do not include information from kSZ power spectrum here, owing to the uncertainties in the contribution from the postreionization kSZ signal to the total kSZ power spectrum. In the future, however, our understanding about the postreionization kSZ signal is expected to improve, thanks to the synergies between CMB and galaxy surveys. Another potential approach is to use the cross-correlation between CMB and galaxy surveys for "de-kSZing" the postreionization kSZ signal [72].

Besides the kSZ measurements, the high-redshift measurements of quasars [recently, [73,74]] from JWST (for a review, see [13]), the upcoming 21 cm measurements from experiments like HERA and SKA [75,76], and the cross-correlation between multiple probes [for example, [77–79]] are all expected to significantly enhance our understanding of the physics of EoR in the next decade. The kSZ results are also expected to improve with the upcoming low-noise multifrequency CMB datasets, namely from the full-depth SPT-3G and SPT-3G+ [39,40,80], Simons Observatory [81], CCAT [82], and CMB-S4 [83] surveys, which all cover a much wider sky area compared to this work. Interpretation of results from the future measurements will necessitate the development of more kSZ simulations like 21 cmFAST [84] and AMBER [46], and also new and multiple realizations of the correlated extragalactic skies like AGORA [33], SEHGAL [85], and WEBSKY [86]. The combination of kSZ 4-point function measurements from the upcoming surveys along with high-significance measurements of the kSZ power spectrum [RO23] and optical depth measurements from LITEBIRD [87] can help to break degeneracies between $z^{\mathrm{mid}}_{\mathrm{re}}$ and $\Delta z_{\mathrm{re},50}$ [31], forming a powerful probe of the epoch of reionization. This work forms a key first step toward such future high precision measurements.

Acknowledgments—We thank all the three anonymous referees for their detailed and valuable feedback that has helped in shaping the manuscript better. S. R. acknowledges support by the Illinois Survey Science Fellowship from the Center for AstroPhysical Surveys at the National Center for Supercomputing Applications. This work made use of the following computing resources: Illinois Campus Cluster, a computing resource that is operated by the

Illinois Campus Cluster Program (ICCP) in conjunction with the National Center for Supercomputing Applications (NCSA) and which is supported by funds from the University of Illinois at Urbana-Champaign; the computational and storage services associated with the Hoffman2 Shared Cluster provided by UCLA Institute for Digital Research and Education's Research Technology Group; and the computing resources provided on Crossover, a high-performance computing cluster operated by the Laboratory Computing Resource Center at Argonne National Laboratory. The South Pole Telescope program is supported by the National Science Foundation (NSF) through grant OPP-1852617. Partial support is also provided by the Kavli Institute of Cosmological Physics at the University of Chicago. Work at Argonne National Lab is supported by UChicago Argonne LLC, Operator of Argonne National Laboratory (Argonne). Argonne, a U.S. Department of Energy Office of Science Laboratory, is operated under Contract No. DE-AC02-06CH11357.

Data availability—The data files and plotting scripts used in this work are available from [88].

[1] R. A. Sunyaev and Y. B. Zeldovich, Mon. Not. R. Astron. Soc. **190**, 413 (1980).
[2] E.-M. Mueller, F. de Bernardis, R. Bean, and M. D. Niemack, Astrophys. J. **808**, 47 (2015).
[3] F. Bianchini and A. Silvestri, Phys. Rev. D **93**, 064026 (2016).
[4] L. Knox, R. Scoccimarro, and S. Dodelson, Phys. Rev. Lett. **81**, 2004 (1998).
[5] M. McQuinn, S. R. Furlanetto, L. Hernquist, O. Zahn, and M. Zaldarriaga, Astrophys. J. **630**, 643 (2005).
[6] O. Zahn, C. L. Reichardt, L. Shaw *et al.*, Astrophys. J. **756**, 65 (2012).
[7] C. L. Reichardt, in Understanding the Epoch of Cosmic Reionization: Challenges and Progress, *Astrophysics and Space Science Library* Vol. 423, edited by A. Mesinger (Springer, Cham, 2016), p. 227.
[8] T. R. Choudhury, Gen. Relativ. Gravit. **54**, 102 (2022).
[9] D. Jain, T. R. Choudhury, S. Raghunathan, and S. Mukherjee, Mon. Not. R. Astron. Soc. **530**, 35 (2024).
[10] R. H. Becker, X. Fan, R. L. White *et al.*, Astron. J. **122**, 2850 (2001).
[11] X. Fan, C. L. Carilli, and B. Keating, Annu. Rev. Astron. Astrophys. **44**, 415 (2006).
[12] B. E. Robertson, R. S. Ellis, J. S. Dunlop, R. J. McLure, and D. P. Stark, Nature (London) **468**, 49 (2010).
[13] B. E. Robertson, Annu. Rev. Astron. Astrophys. **60**, 121 (2022).
[14] M. Zaldarriaga, Phys. Rev. D **55**, 1822 (1997).
[15] R. Adam, N. Aghanim, M. Ashdown *et al.* (Planck Collaboration), Astron. Astrophys. **596**, A108 (2016).
[16] N. Hand, G. E. Addison, E. Aubourg *et al.*, Phys. Rev. Lett. **109**, 041101 (2012).
[17] J. C. Hill, S. Ferraro, N. Battaglia, J. Liu, and D. N. Spergel, Phys. Rev. Lett. **117**, 051301 (2016).
[18] V. Calafut, P. Gallardo, E. Vavagiakis *et al.*, Phys. Rev. D **104**, 043502 (2021).
[19] E. Schaan, S. Ferraro, S. Amodeo *et al.*, Phys. Rev. D **103**, 063513 (2021).
[20] E. Schiappucci, F. Bianchini, M. Aguena *et al.*, Phys. Rev. D **107**, 042004 (2023).
[21] M. Mallaby-Kay, S. Amodeo, J. C. Hill *et al.*, Phys. Rev. D **108**, 023516 (2023).
[22] P. La Plante, J. Sipple, and A. Lidz, Astrophys. J. **928**, 162 (2022).
[23] C. Dvorkin and K. M. Smith, Phys. Rev. D **79**, 043003 (2009).
[24] L. D. Shaw, D. H. Rudd, and D. Nagai, Astrophys. J. **756**, 15 (2012).
[25] N. Battaglia, A. Natarajan, H. Trac, R. Cen, and A. Loeb, Astrophys. J. **776**, 83 (2013).
[26] S. Raghunathan and Y. Omori, Astrophys. J. **954**, 83 (2023).
[27] C. L. Reichardt, S. Patil, P. A. R. Ade *et al.*, Astrophys. J. **908**, 199 (2021).
[28] A. Gorce, M. Douspis, and L. Salvati, Astron. Astrophys. **662**, A122 (2022).
[29] K. M. Smith and S. Ferraro, Phys. Rev. Lett. **119**, 021301 (2017).
[30] S. Ferraro and K. M. Smith, Phys. Rev. D **98**, 123519 (2018).
[31] M. A. Alvarez, S. Ferraro, J. C. Hill, R. Hložek, and M. Ikape, Phys. Rev. D **103**, 063518 (2021).
[32] T. Okamoto and W. Hu, Phys. Rev. D **67**, 083002 (2003).
[33] Y. Omori, arXiv:2212.07420.
[34] S. Padin, Z. Staniszewski, R. Keisler *et al.*, Appl. Opt. **47**, 4418 (2008).
[35] J. E. Carlstrom, P. A. R. Ade, K. A. Aird *et al.*, Publ. Astron. Soc. Pac. **123**, 568 (2011).
[36] G. L. Pilbratt, J. R. Riedinger, T. Passvogel *et al.*, Astron. Astrophys. **518**, L1 (2010).
[37] M. J. Griffin, A. Abergel, A. Abreu *et al.*, Astron. Astrophys. **518**, L3 (2010).
[38] J. E. Austermann, K. A. Aird, J. A. Beall *et al.*, Proc. SPIE Int. Soc. Opt. Eng. **8452**, 84521E (2012).
[39] B. A. Benson, P. A. R. Ade, Z. Ahmed *et al.*, Proc. SPIE Int. Soc. Opt. Eng. **9153**, 91531P (2014).
[40] A. N. Bender, P. A. R. Ade, Z. Ahmed *et al.*, Proc. SPIE Int. Soc. Opt. Eng. **10708**, 1070803 (2018).
[41] J. A. Sobrin, A. J. Anderson, A. N. Bender *et al.*, Astrophys. J. Suppl. Ser. **258**, 42 (2022).
[42] J. W. Henning, J. T. Sayre, C. L. Reichardt *et al.*, Astrophys. J. **852**, 97 (2018).
[43] M. P. Viero, C. L. Reichardt, B. A. Benson *et al.*, Astrophys. J. **881**, 96 (2019).
[44] See Supplemental Material at http://link.aps.org/supplemental/10.1103/PhysRevLett.133.121004 for details, which includes Refs. [25–27,29,33,42,43,45–65].
[45] J.-F. Cardoso, M. Le Jeune, J. Delabrouille, M. Betoule, and G. Patanchon, IEEE J. Sel. Top. Signal Process. **2**, 735 (2008).
[46] H. Trac, N. Chen, I. Holst, M. A. Alvarez, and R. Cen, Astrophys. J. **927**, 186 (2022).

[47] K. K. Schaffer, T. M. Crawford, K. A. Aird *et al.*, Astrophys. J. **743**, 90 (2011).
[48] D. Dutcher, L. Balkenhol, P. A. R. Ade *et al.*, Phys. Rev. D **104**, 022003 (2021).
[49] M. R. Calabretta and E. W. Greisen, Astron. Astrophys. **395**, 1077 (2002).
[50] G. P. Holder, M. P. Viero, O. Zahn *et al.*, Astrophys. J. Lett. **771**, L16 (2013).
[51] M. P. Viero, L. Wang, M. Zemcov *et al.*, Astrophys. J. **772**, 77 (2013).
[52] A. Benoit-Lévy, T. Déchelette, K. Benabed, J.-F. Cardoso, D. Hanson, and S. Prunet, Astron. Astrophys. **555**, A37 (2013).
[53] S. Raghunathan, G. P. Holder, J. G. Bartlett, S. Patil, C. L. Reichardt, and N. Whitehorn, J. Cosmol. Astropart. Phys. 11 (2019) 037.
[54] M. Archipley *et al.* (to be published).
[55] K. Kornoelje *et al.* (to be published).
[56] S. Raghunathan, Astrophys. J. **928**, 16 (2022).
[57] A. Lewis, A. Challinor, and A. Lasenby, Astrophys. J. **538**, 473 (2000).
[58] M. S. Madhavacheril, K. M. Smith, B. D. Sherwin, and S. Naess, J. Cosmol. Astropart. Phys. 05 (2021) 028.
[59] A. Klypin, G. Yepes, S. Gottlöber, F. Prada, and S. Heß, Mon. Not. R. Astron. Soc. **457**, 4340 (2016).
[60] N. Chen, H. Trac, S. Mukherjee, and R. Cen, Astrophys. J. **943**, 138 (2023).
[61] W. L. K. Wu, L. M. Mocanu, P. A. R. Ade *et al.*, Astrophys. J. **884**, 70 (2019).
[62] M. Millea, C. M. Daley, T. L. Chou *et al.*, Astrophys. J. **922**, 259 (2021).
[63] M. Remazeilles, J. Delabrouille, and J.-F. Cardoso, Mon. Not. R. Astron. Soc. **410**, 2481 (2011).
[64] A. van Engelen, S. Bhattacharya, N. Sehgal, G. P. Holder, O. Zahn, and D. Nagai, Astrophys. J. **786**, 13 (2014).
[65] B. M. Swinyard, P. Ade, J. P. Baluteau *et al.*, Astron. Astrophys. **518**, L4 (2010).
[66] P. A. R. Ade, N. Aghanim, M. Arnaud *et al.* (Planck Collaboration), Astron. Astrophys. **594**, A24 (2016).
[67] T. Namikawa, D. Hanson, and R. Takahashi, Mon. Not. R. Astron. Soc. **431**, 609 (2013).
[68] S. J. Osborne, D. Hanson, and O. Doré, J. Cosmol. Astropart. Phys. 03 (2014) 024.
[69] N. Sailer, E. Schaan, S. Ferraro, O. Darwish, and B. Sherwin, Phys. Rev. D **104**, 123514 (2021).
[70] A. Manzotti, K. T. Story, W. L. K. Wu *et al.*, Astrophys. J. **846**, 45 (2017).
[71] P. A. R. Ade, Z. Ahmed, M. Amiri *et al.*, Phys. Rev. D **103**, 022004 (2021).
[72] S. Foreman, S. C. Hotinli, M. S. Madhavacheril, A. van Engelen, and C. D. Kreisch, Phys. Rev. D **107**, 083502 (2023).
[73] P. Dayal, M. Volonteri, J. E. Greene *et al.*, arXiv:2401.11242.
[74] J. B. Muñoz, J. Mirocha, J. Chisholm, S. R. Furlanetto, and C. Mason, arXiv:2404.07250.
[75] A. Liu and J. R. Shaw, Publ. Astron. Soc. Pac. **132**, 062001 (2020).
[76] Z. Abdurashidova, T. Adams, J. E. Aguirre *et al.* (The HERA Collaboration), Astrophys. J. **945**, 124 (2023).
[77] T. Namikawa, A. Roy, B. D. Sherwin, N. Battaglia, and D. N. Spergel, Phys. Rev. D **104**, 063514 (2021).
[78] P. La Plante, J. Mirocha, A. Gorce, A. Lidz, and A. Parsons, Astrophys. J. **944**, 59 (2023).
[79] I. Georgiev, A. Gorce, and G. Mellema, Mon. Not. R. Astron. Soc. **528**, 7218 (2024).
[80] A. J. Anderson, P. Barry, A. N. Bender *et al.*, Proc. SPIE Int. Soc. Opt. Eng. **12190**, 35 (2022).
[81] Simons Observatory Collaboration, J. Cosmol. Astropart. Phys. 02 (2019) 056.
[82] N. F. Cothard, S. K. Choi, C. J. Duell *et al.*, J. Low Temp. Phys. **199**, 898 (2020).
[83] K. Abazajian, G. Addison, P. Adshead *et al.* (CMB-S4 Collaboration), arXiv:1907.04473.
[84] A. Mesinger, S. Furlanetto, and R. Cen, Mon. Not. R. Astron. Soc. **411**, 955 (2011).
[85] N. Sehgal, P. Bode, S. Das, C. Hernandez-Monteagudo, K. Huffenberger, Y.-T. Lin, J. P. Ostriker, and H. Trac, Astrophys. J. **709**, 920 (2010).
[86] G. Stein, M. A. Alvarez, J. R. Bond, A. van Engelen, and N. Battaglia, J. Cosmol. Astropart. Phys. 10 (2020) 012.
[87] E. Allys, K. Arnold, J. Aumont *et al.* (LiteBIRD Collaboration), Prog. Theor. Exp. Phys. **2023**, 042F01 (2023).
[88] https://github.com/sriniraghunathan/kSZ_4pt_SPT_SPIRE.